Supporting information

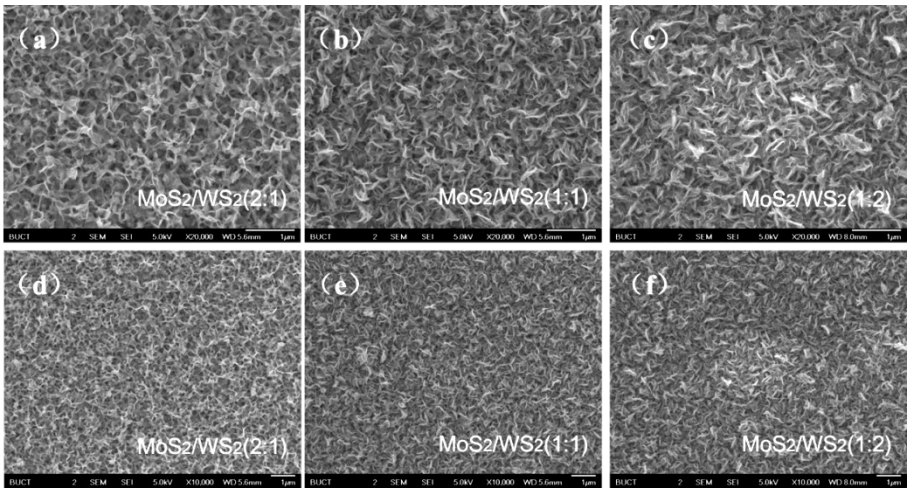

Fig.S1 SEM images of MoS_2/WS_2 catalyst with different Mo:W ratios.(a) and (d) Mo:W=2:1; (b) and (e) Mo:W=2:1; (c) and (f) Mo:W=2:1

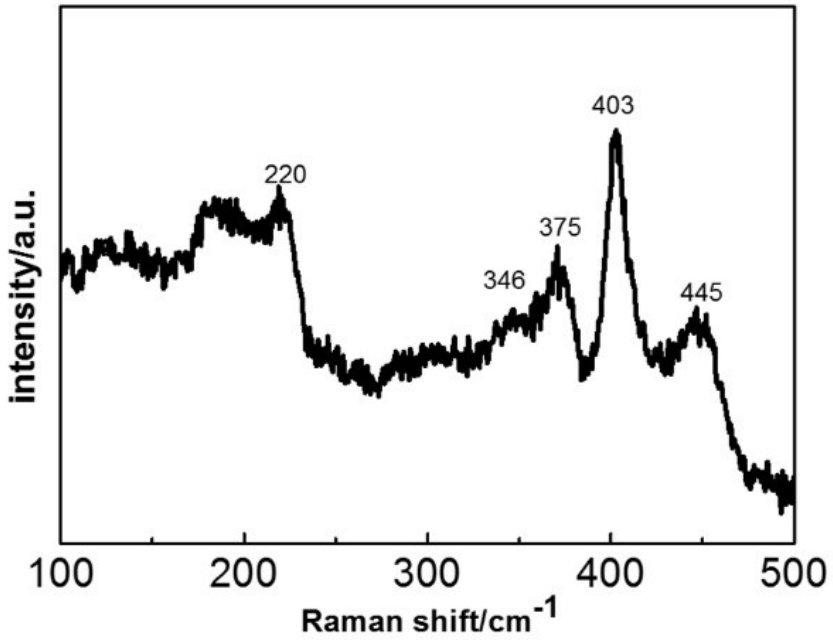

Fig.S2 Raman spectra of MoS_2/WS_2 (1:1)

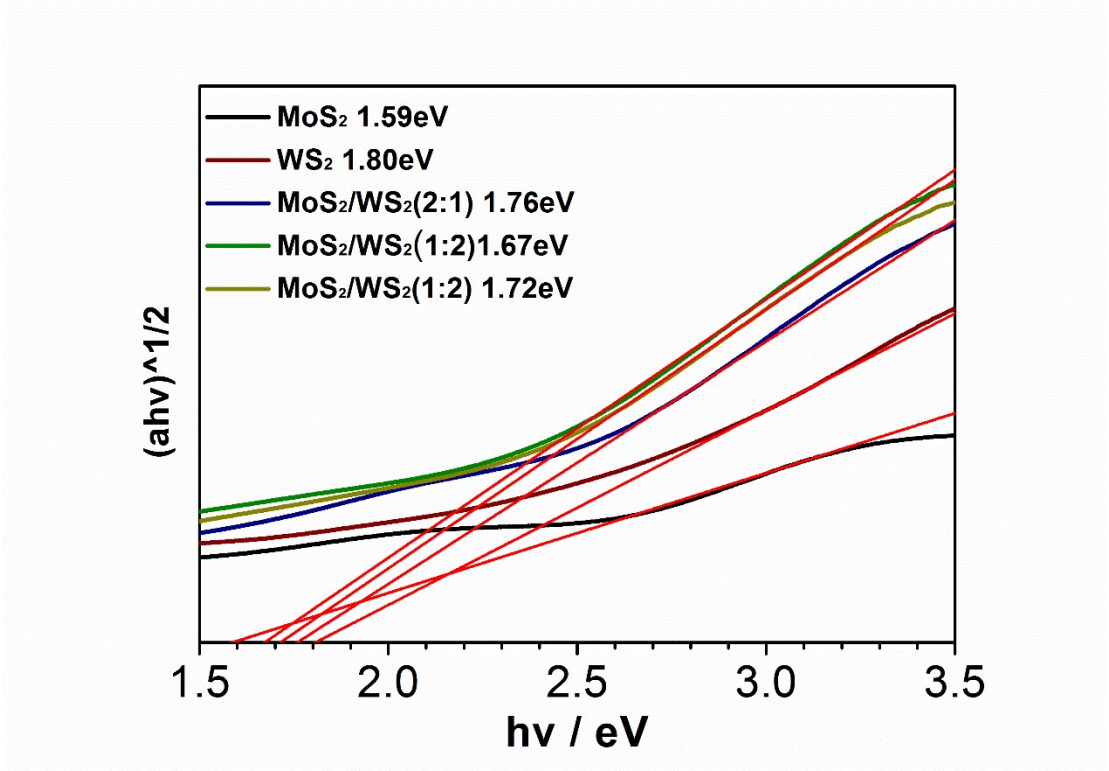

Fig.S3 The band gap of the MoS_2, WS_2, and MoS_2/WS_2 catalyst with different Mo:W mole ratios

The optical band gap (Eg) of the samples was calculated using the Tauc's method. [1] According to this method, the plot of $[ahv]^n$ against hv shows a linear region just above the optical absorption edge, where n = 2 is used for the direct allowed transition, n = 1/2 for the indirect allowed transition, and hv is the photon energy (eV). Bulk or fewer 2H-MoS_2 is a semiconductor with an indirect band gap of ~1.2 eV, and the nature of the band gap changes from indirect to direct when thickness is reduced to be a single layer (~1.9 eV). [2] We estimated the band gap using n = 1/2 for the indirect allowed transition, which was fitted for the fewer layer MoS_2 or WS_2 nanosheets. Hence, in the Tauc plot shown in Figure S3, n = 1/2 was employed, which clearly yields a satisfactory linearity for all the WS_2, MoS_2 and MoS_2/WS_2 samples. The band gap Eg is derived from the intercept of this straight line with the photon energy axis at $[ahv]^{1/2}=0$. The resulting Eg values for WS_2, MoS_2 and MoS_2/WS_2 are shown in Fig.S3. In this context, both WS_2 and MoS_2 exhibit a small increase in the band gap. The increase in the band gap is properly attributed to the effect of the Eg of In_2S_3 (~2.4 eV) derived of ITO under hydrothermal condition.

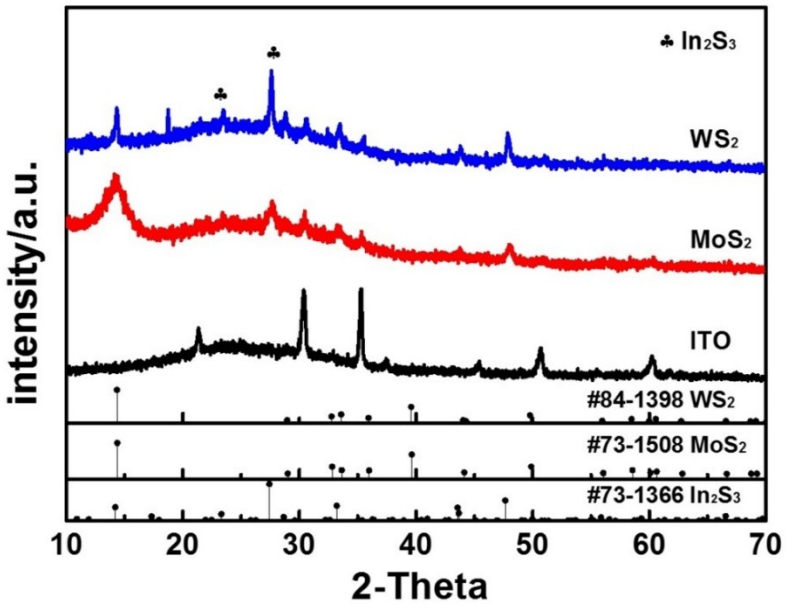

Fig.S4 XRD patterns of the pristine WS2 and MoS2 grown on ITO under hydrothermal condition

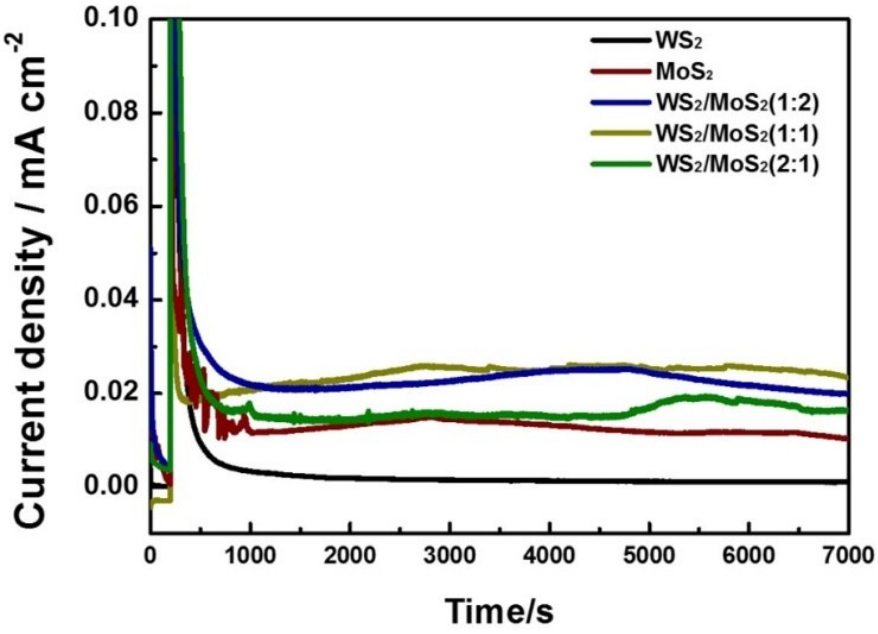

Fig.S5 I-t plot for stability testing of the nanostructured MoS_2, WS_2 and MoS_2/WS_2 of different mole ratio at 0.372 V (vs RHE). Light source: Xenon lamp (300W) (0.50M H_2SO_4)

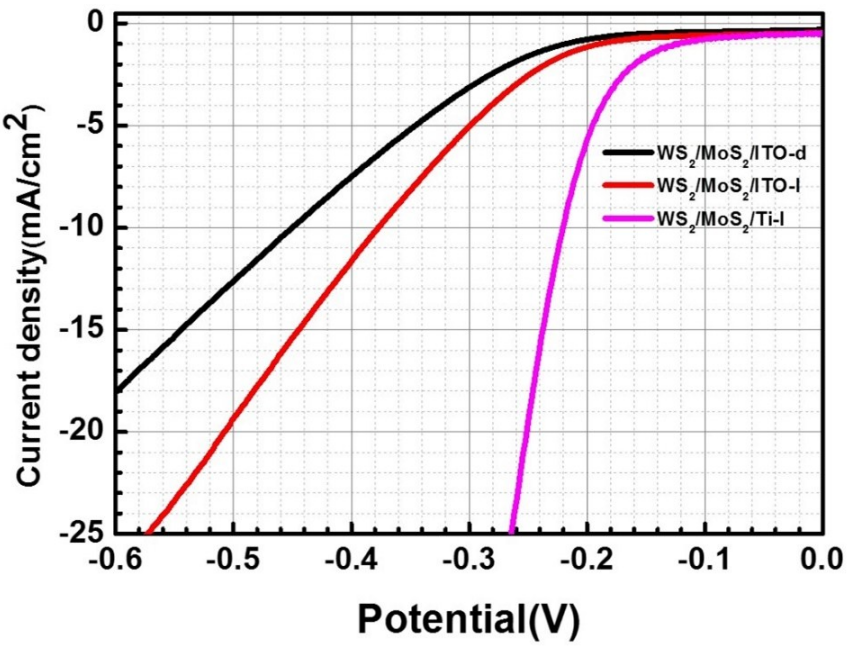

Fig.S6 J-V curves of cathodic polarization of MoS_2/WS_2 catalysts on ITO and MoS_2/WS_2 catalysts on Ti in dark and under simulated solar light (0.5M H_2SO_4)

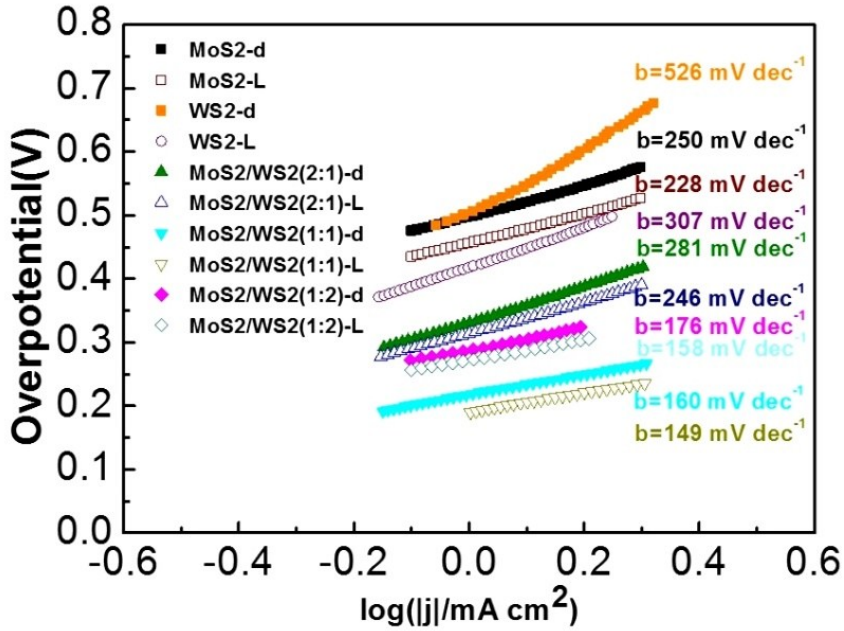

Fig. S7 Tafel plots of as prepared photoelectrocatalysts

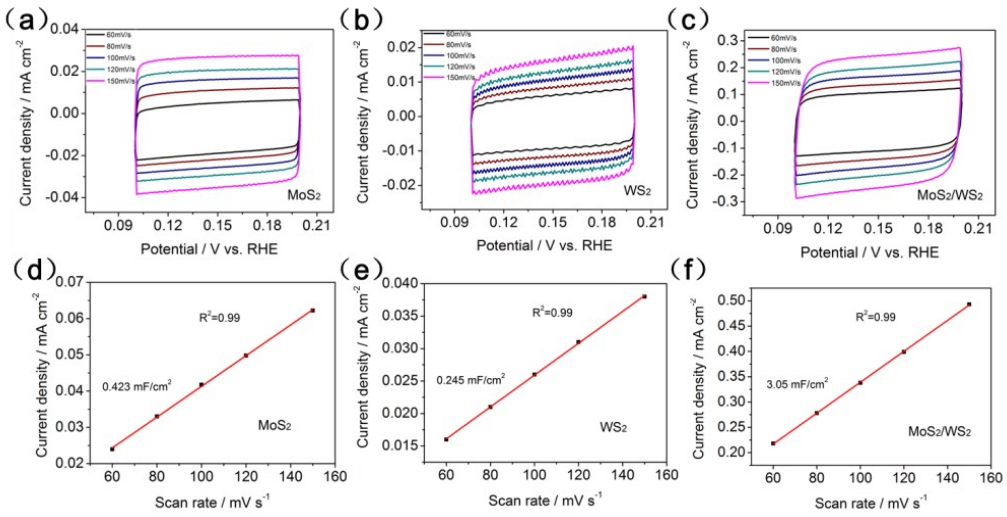

Fig.S8 Electrochemical double-layer capacitance (EDLC) measurements and the corresponding current density-scan rates curve of several electrocatalysts. (a) and (d) MoS_2; (b)and(e) WS_2; (c)and(f) MoS_2/WS_2(1:1),respectively.

The electrochemical double-layer capacitance (EDLE) is determined by the following equation: ic = vCDL; where ic represents the capacitive current, v is the product of the scan rate, and CDL is the electrochemical double-layer capacitance. The electrochemical double-layer capacitance is obtained by the slop of a straight line extracted from the capacitive current as a function of scan rate. [3-5]

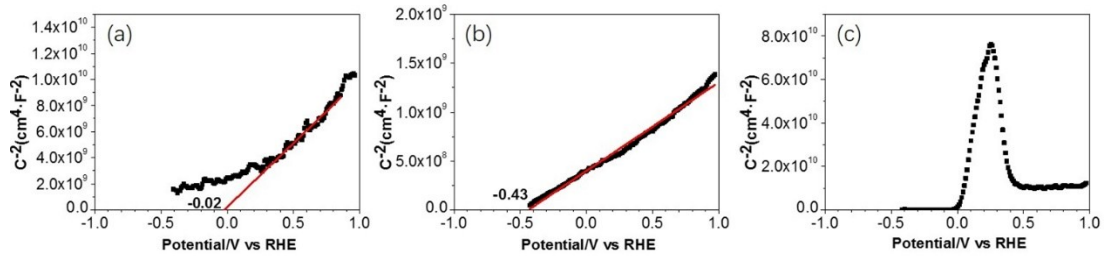

Fig.S9 Mott-Schottky plot of photoelectrodes (a) MoS2; (b) WS2; (c) MoS2/WS2 (1:1), respectively.

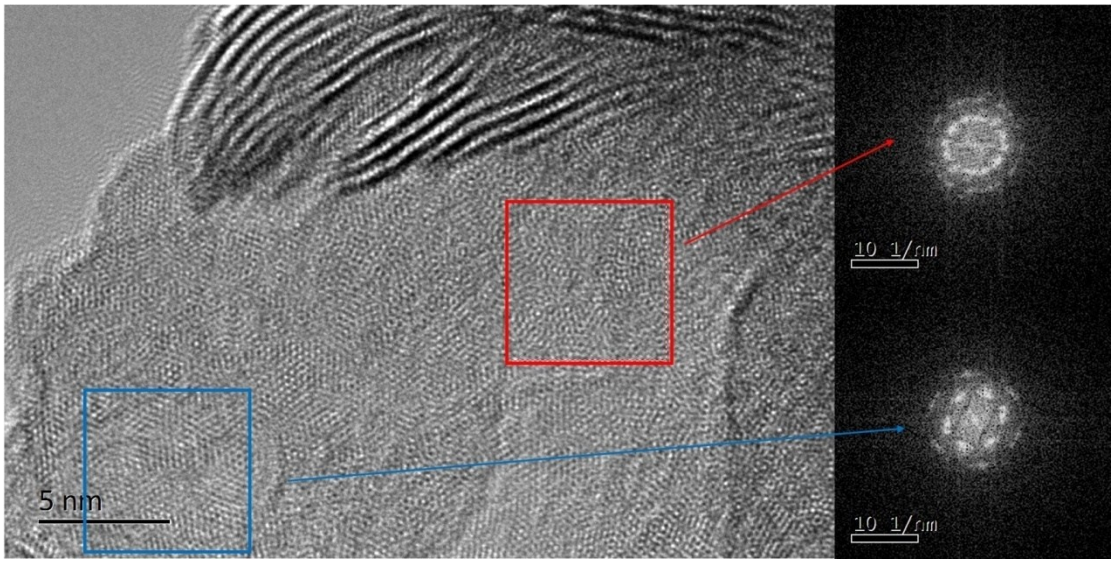

Fig.S10 HRTEM image of MoS_2/WS_2 (1/1) with its corresponding fast Fourier transform (FFT), highlighting the ordered and random orientation of individual building blocks (evidenced by FFT ring pattern)

From the structural viewpoint for HER catalysis, the strongly disordered structure is beneficial to offer more active sites. [6] However, fast interdomain electron transport due to the 2D electron conjugation along the basal surface will be significantly blocked by the disordered structure,[7] and thus leads to poor overall conductivity and further restrict the HER process. Hence, a moderate degree of disorder with a certain periodic arrangement of nanodomains should be adjusted to compromise the contradictory relation between active sites and conductivity. In this special hierarchical structure, controllable disorder of nanostrucuture can be achieved by W-dopping MoS_2 hybrid, which offers the opportunity to tune the active site numbers. During reaction, W probably located on substitutional sites, will tend to migrate toward the free surfaces and edges of the MoS_2, which changes on the rotated surface interlayers.

Actually, for MoS_2/WS_2 (1/1) sample, ordered and disordered domains coexisted in the atomic arranging manners. The coexistence of ordered and disordered domains were confirmed by HRTEM image (SI Fig.S10). As shown in above HRTEM image (SI

Fig.S10), both disordered and ordered nanodomain are observed, as indicated by the red and blue boxes, respectively.

As shown in Fig.S10, some nanodomain are observed as the rotation of overlapped hexagonal networks between individual MoS_2 layers,[7] which is a kind of disordered structure. In order to directly estimate the extent of disorder for the MoS_2/ WS_2 sample, fast Fourier transform (FFT) was applied to show splitting whose angle corresponds to the degrees of rotation, thus reflecting the degrees of disorder[8-12] In addition, the degree of disorder can be evaluated by the angle determined by a diffraction arc length and the central spot,[5] and the different diffraction arc length indicates the different periodic arrangements of nanodomains.

As shown in the upper right of Fig. S10, the FFT patterns (enclosed by red box) showed a set of concentric rings instead of sharp spots as a result of the strongly disordered arrangement of nanodomains. Furthermore, the image obtained with the other part of the sample, enclosed by blue box, FFT pattern, shown in the lower right of Fig.S10, is observed to possess six diffraction arcs with little arc length, indicating an almost single layer of nanodomains with a good periodic arrangement. Additionally, WS_2 has been verified to be highly crystallized as compared with MoS_2. [13] In this work, the XRD spectrum clearly shows that the highly crystallized WS_2 and poorly crystallized MoS_2 coexist in the hybrid. It is inferred that the as-obtained MoS_2/WS_2 nanosheet of mole ratio of 1/1 possesses simultaneously intrinsic conductivity and defects, hence being anticipated to have enhanced electrocatalytic activity for HER process.

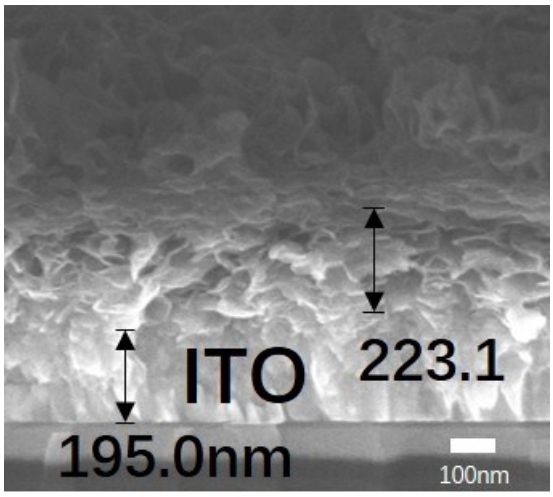

Fig.S11 SEM images of the cross-section for MoS_2/WS_2 (1:1) catalyst

In a typical photocatalytic experiment, MoS_2/WS_2 grown uniformly on 8cm^2 area of the ITO substrate was suspended in 20 ml 0.50 M H_2SO_4 solution. The thickness of the MoS_2/WS_2 layer is ~223.1nm (Fig.S11).The opening of the reactor was sealed with a silicone rubber septum. Bubbling N_2 gas is required to remove air in the reactant mixture and to ensure the anaerobic conditions of the reaction system. And then, the reaction system was irradiated by a 300-W Xe lamp with a cutoff filter of 420 nm for H_2 evolution. The amount of hydrogen evolution was measured using gas chromatography ((GC- 7920, TCD detector), and the hydrogen production rate is 0.049ml h^{-1}. For comparison with the previous studies, we have to convert it to μmol g^{-1} h^{-1}, a customary unit used for hydrogen production rate. The hydrogen production rate is determined by the following equation:

$$\nu\ (H_2)\ = \frac{n}{tm} \quad (1);\ m = S_{MoS2/WS2} \times h \times \rho_{MoS2} \quad (2);\quad V = \frac{M}{\rho} n \quad (3)$$

where $\nu(H_2)$ represents the hydrogen production rate /μmol g^{-1} h^{-1}, t is the operation time (hour), m is the mass weight of the MoS_2/WS_2 which is estimated by equation (2) wherein, $S_{MoS2/WS2}$ is the surface areas of MoS_2/WS_2/ITO(8cm^2), h represent the thickness of the MoS_2/WS_2 layer(223×10^{-4}cm), and ρ_{MoS2} is the density of MoS_2 (4.8g cm^{-3}) (the density of MoS_2 is used in the equation (2) since the amount of WS_2 in

hybrid is so small that it can be ignored. n is the moles of the produced H_2 which is calculated from the equation (3), V is hydrogen gas volume (0.049ml h^{-1}), M is the molar mass of H_2 (2), ρ is the density of the H_2 (0.899 g cm^{-3}). Noteworthy is, the estimated mass of MoS_2/WS_2 is greater than the actual mass because the MoS_2/WS_2 structure is hierarchical rather than solid, thus leading to the lowest estimate for H_2 evolution production.

Table S1 Comparison of Hydrogen Evolution Data of WS_2/MoS_2 Composites Compared with Few of the Literature Reports

catalyst	activity (μmol h−1 g−1)	reaction conditions	Ref
WS_2/MoS_2/Au	1.819	0.5 M H_2SO_4（a 300 W Xe lamp；λ>420 nm）	14（2016）
CdS/WS_2	373.41	Na_2SO_4 aqueous solution (0.5 M) （300 W Xe lamp；λ> 420 nm）	15（2016）
g-C_3N_4/WS2	101	Methanol： water （1:3) （300 W xenon arc lamp ;λ≥420 nm)	16（2015）
$MoS_2@Cu_2O$	562.5	methanol/water(1:3) 350 W Xe arc lamp (λ≥420 nm) at a bias of −0.1 V vs. SCE	17（2014）

MoS_2 QDs	2070	10% (v/v) triethanolamine (TEOA) aqueous solution (300 W xenon arc lamp ;λ≥420 nm)	18 (2017)
TiO2/1T-WS_2	2570	methanol/water(1:3)（300 W xenon arc lamp)	19 (2014)
AgInZnS/MoS_2	944	aqueous solution containing 10% lactic acid(300 W xenon arc lamp ;λ≥420 nm)	20 (2017)
WS_2/MoS_2	>2065	0.50 M H_2SO_4/lactic acid solution(300 W xenon arc lamp ;λ≥420 nm)	This work

1. K. M. Reddy, S. V. Manorama and A. R. Reddy, Mate. Chem. Phys., 2003, 78, 239-245.
2. B. Radisavljevic, A. Radenovic, J. Brivio, V. Giacometti and A. Kis, Nature Nanotechnology, 2011, 6, 147-150.
3. S. Trasatti and O. A. Petrii, Pure Appl. Chem., 1991, 63, 711–734.
4. J. D. Benck, Z. Chen, L. Y. Kuritzky, A. J. Forman and T. F. Jaramillo, ACS Catalysis, 2012, 2, 1916-1923.
5. R. Boggio, A. Garugati and S. Trasatti, J. Appl. Electrochem., 1987, 17, 828-840.
6. H. V. Swygenhoven, Science, 2002, 296, 66-67.
7. J.-F. Xie, H. Zhang, S. Li, R.-X. Wang, X. Sun, M. Zhou, J.-F. Zhou, X.-W. Lou and Y. Xie, Advanced materials, 2013, 25, 5807-5813.
8. S. Najmaei, Z. Liu, W. Zhou, X. Zou, G. Shi, S. Lei, B. I. Yakobson, J.-C. Idrobo, P. M. Ajayan and J. Lou, Nat. Mater. , 2013, 12, 754-759.
9. K. Kim, Z. Lee, W. Regan, C. K. Kisielowski, M. F. Crommie and A. Zettl, ACS Nano,

2011, 5, 2142-2146.

10. P. Y. Huang, C. S. Ruiz-Vargas, A. M. van der Zande, W. S. Whitney, M. P. Levendorf, J. W. Kevek, S. Garg, J. S. Alden, C. J. Hustedt, Y. Zhu, J. Park, P. L. McEuen and D. A. Muller, Nature, 2011, 469, 389-392.
11. A. L. Gibb, N. Alem, J. H. Chen, K. J. Erickson, J. Ciston, A. Gautam, M. Linck and A. Zettl, J. Am. Chem. Soc., 2013, 135, 6758-6761.
12. J.-H. An, E. Voelkl, J. W. Suk, X. S. Li, C. W. Magnuson, L. F. Fu, P. Tiemeijer, M. Bischoff, B. Freitag, E. Popova and R. S. Ruoff, ACS Nano, 2011, 5, 2433-2439.
13. G. Alonso-Núñez, R. Huirache-Acuña, F. Paraguay-Delgado, J. A. Lumbreras, R. García-Alamilla, A. Castillo-Mares, R. Romero, R. Somanathan and R. R. Chianelli, Catalysis Letters, 2009, 130, 318-326.
14. J. Shi, R. Tong, X. Zhou, Y. Gong, Z. Zhang, Q. Ji, Y. Zhang, Q. Fang, L. Gu, X. Wang, Z. Liu and Y. Zhang, Adv Mater, 2016, 28, 10664-10672.
15. Y. Zhong, G. Zhao, F. Ma, Y. Wu and X. Hao, Applied Catalysis B: Environmental, 2016, 199, 466-472.
16. M. S. Akple, J. Low, S. Wageh, A. A. Al-Ghamdi, J. Yu and J. Zhang, Applied Surface Science, 2015, 358, 196-203.
17. Y.-F. Zhao, Z.-Y. Yang, Y.-X. Zhang, L. Jing, X. Guo, Z.-T. Ke, P.-W. Hu, G.-X. Wang, Y.-M. Yan and K.-N. Sun, J. Phys. Chem. C, 2014, 118, 14238-14245.
18. X. Hao, Z. Jin, H. Yang, G. Lu and Y. Bi, Applied Catalysis B: Environmental, 2017, 210, 45-56.
19. B. Mahler, V. Hoepfner, K. Liao and G. A. Ozin, J Am Chem Soc, 2014, 136, 14121-14127.
20. T. Huang, W. Chen, T.-Y. Liu, Q.-L. Hao and X.-H. Liu, International Journal of Hydrogen Energy, 2017, 42, 12254-12261.